Applied Catalysis B: Environmental 307 (2022) 121197

Contents lists available at ScienceDirect

Applied Catalysis B: Environmental

journal homepage: www.elsevier.com/locate/apcatb

Kinetics of nitrogen-, oxygen- and sulfur-containing compounds hydrotreating during co-processing of bio-crude with petroleum stream

Cheng Zhu [a], Oliver Y. Gutiérrez [b], Daniel M. Santosa [a], Matthew Flake [a], Roland Weindl [c], Igor Kutnyakov [a], Hui Shi [c], Huamin Wang [a,*]

[a] Energy and Environment Directorate, Pacific Northwest National Laboratory, 902 Battelle Boulevard, Richland, WA 99352, United States
[b] Physical and Computational Sciences Directorate, Pacific Northwest National Laboratory, 902 Battelle Boulevard, Richland, WA 99352, United States
[c] Department of Chemistry and Catalysis Research Center, Technical University of Munich, 85747 Garching, Germany

ARTICLE INFO

Keywords:
Fatty acid amides
Hydrodenitrogenation
Hydrodeoxygenation
Hydrodesulfurization
Co-processing
HTL bio-crude
Hydrotreating

ABSTRACT

The rational selection of catalysts and process parameters for co-processing biomass- and waste-derived bio-crudes with petroleum streams requires detailed reaction networks and kinetics of the conversion of heteroatom-containing compounds existed in both kinds of feedstocks. We provide the kinetics and reaction networks for the hydrotreating of N,N-diethyldodecanamide and N-methyldodecanamide, model compounds of major components in bio-crudes from hydrothermal liquefaction of wet waste. Their conversion undergoes via two pathways over sulfided $NiMo/Al_2O_3$ catalyst: deoxygenation followed by denitrogenation of the amine intermediate (DO pathway), and denitrogenation followed by deoxygenation of the alkanol intermediate (DN pathway)—with the DO pathway dominant over the DN pathway. H_2S inhibits the deoxygenation step and promotes the denitrogenation step in the DO pathway. The amine intermediate inhibits the amide conversion, with weaker effects on the conversion of secondary amide than on the tertiary amide. The kinetics of hydrotreating of several model compounds representing the main species during co-processing indicate that the removal of nitrogenous species, which are in large quantities and of varying structures, remains the main challenge (compared with S- and O-removal) for co-processing.

1. Introduction

Renewable energies are receiving increasing attention and demand to address the societal and economic challenges associated with the use of fossil fuels and their environmental impact [1,2]. Biomass-derived fuels are a major source of renewable energy due to the large availability of biomass feedstocks and the advancement of biomass conversion technologies [3,4]. Hydrothermal liquefaction (HTL) offers a relatively straightforward process to convert wet wastes and biomass into liquid fuels and carbon-based chemicals [5,6]. However, HTL-derived bio-crudes do not meet the petroleum fuel standards and require upgrading to improve their physical and chemical properties in order to produce fuel range hydrocarbons [7]. Upgrading bio-crudes can be done with hydrotreating, which is a common and well-established upgrading technology already available in existing oil refineries [8,9], and bio-crude hydrotreating can be performed in a standalone biorefinery or an existing petroleum refinery with co-processing [10,11]. Co-processing can utilize existing infrastructure, thereby reducing capital costs [12,13]. Extensive work has been reported on the co-processing of vegetable oils [14], animal fats [15], waste cooking oils [16], and HTL bio-crude [17] with refinery streams in hydrotreating and/or hydrocracking, as well as raw pyrolysis bio-oil [18,19] with vacuum gas oil (VGO) in fluid catalytic cracking (FCC).

HTL bio-crudes from wet wastes or algae contain a wide variety of chemicals, including fatty acids, phenolics, esters, alcohols, aliphatic hydrocarbons, aromatics, and nitrogenous components [20]. The elemental compositions of a typical HTL bio-crude from sewage sludge and a typical petroleum crude oil reported in the literature are compared in Table 1. Unlike pyrolysis and HTL bio-oils from lignocellulosic biomass such as forest residues, which are normally low in sulfur and nitrogen, HTL bio-crude from sewage sludge or algae has an abundance of nitrogen compounds derived from a large amount of protein present in the feedstock [21,22]. These nitrogenous components are of varied structures and composed of long-chain fatty acid amides, heterocyclic amines, and amino acids [23]. Therefore, understanding the hydrotreating kinetics and reaction networks of these heteroatom-containing

* Corresponding author.
E-mail address: huamin.wang@pnnl.gov (H. Wang).

https://doi.org/10.1016/j.apcatb.2022.121197
Received 22 November 2021; Received in revised form 10 January 2022; Accepted 6 February 2022
Available online 9 February 2022

Table 1
Elemental composition of HTL bio-crude and petroleum stream (VGO) [32–35].

Property	Typical HTL bio-crudes from sewage sludge	Typical VGO
C (%)	61.5–79.3	83.0–87.0
H (%)	8.5–12.0	10.0–14.0
O (%)	10.8–20.2	0.05–1.5
N (%)	4.2–9.8	0.01–2
S (%)	0.1–1.2	0.1–6.0

species is crucial for developing efficient co-processing approaches [24]. Within the major heteroatom-containing compounds found in HTL bio-crudes and petroleum streams, hydrotreating of fatty acids, phenolics, furans, [25,26] thiols and thiophenes (such as thiophenes, benzothiophenes, dibenzothiophenes), [27,28] and amines and cyclic amines (including pyridine derivatives and pyrrole derivatives) [29,30] have been extensively studied. However, there is limited knowledge of the conversion of fatty acid amides—major nitrogen and oxygen-containing component in sewage sludge HTL bio-crudes [31].

Therefore, we studied the hydrodenitrogenation-hydrodeoxygenation (HDN-HDO) kinetics of fatty acid amides over a NiMo sulfide catalyst to determine the corresponding kinetic parameters (reaction rate constants and apparent activity energies) and reaction networks. The influence of H_2S on primary and secondary reactions and the effects of substituting groups in secondary and tertiary amides were investigated. Additionally, we determined the kinetics of other oxygen-, sulfur-, and nitrogen-containing model compounds representing main species in HTL bio-crudes and petroleum streams such as vacuum gas oil (VGO) to compare their hydrodeoxygenation (HDO), hydrodesulfurization (HDS), and hydrodenitrogenation (HDN) reactivities.

2. Experimental method

A commercial sulfided NiMo/γ-Al_2O_3 catalyst was used for the kinetic study of hydrotreating nitrogen-, oxygen- and sulfur-containing model compounds. Model compounds that were used include: N,N-diethyldodecanamide (DEDAD, Tokyo Chemical Industry, > 98%), N-methyldodecanamide (MDAD, Tokyo Chemical Industry, > 98%), N,N-dimethyldodecylamine (DMDAM, Tokyo Chemical Industry, > 96%), N-methyldodecylamine (MDAM, Sigma-Aldrich, 97%), dodecanoic acid (DA, Tokyo Chemical Industry, > 98%), 4-propylphenol (Tokyo Chemical Industry, > 99%), dibenzothiophene (DBT, Acros Organics, 98%), and quinoline (Tokyo Chemical Industry, > 98%).

The model compounds were converted in a bench-scale hydrotreater system (see Fig. S1) [36] containing gas and liquid feeding system, a continuous downflow fixed-bed reactor, and a gas-liquid separation system. The tubular reactor is built of 316 stainless steel tubing with a 7 mL capacity (7.747 mm ID x 152.4 mm L). The liquid reactants and sulfiding agents are pumped into the heated reactor by high-pressure ISCO syringe pumps, while the hydrogen and purging nitrogen flow rates are controlled by mass flow controllers. After the products exited the catalytic reactor, the liquid and gas were separated in pressurized and cooled traps while the liquid products were sampled and analyzed.

The NiMo catalyst was crushed and sieved to 60–100 mesh (0.149–0.25 mm) particle size. In each run, 25 or 50 mg catalyst was diluted with SiC (Kramer Industries, 70 mesh, 0.21 mm) to a total of 7 mL to avoid temperature or concentration gradients that can corrupt the intended kinetic origin of the measured rates and selectivities and to ensure that bed lengths were sufficiently long for plug-flow hydrodynamics. Varying the catalyst particle size, catalyst/SiC dilution ratio, and catalyst amount did not influence measured conversion rates and product selectivity, confirming the absence of transport artifacts in the kinetic measurement.

Before each series of experiments, the fresh catalyst bed was sulfided in situ using a solution of 35 wt% di-tert-butyl-disulfide (DTBDS, Sigma-Aldrich, 97%) in decane (Sigma-Aldrich, > 99%) at 5.3 MPa under flowing H_2 at 400 °C. Each hydrotreating test was conducted at 5.3 MPa total pressure with 10 kPa model compound, 280 kPa tetradecane (as solvent, Tokyo Chemical Industry, > 99%), 16 kPa hexadecane (as GC internal standard, Acros Organics, 99%), 0 or 30 kPa H_2S, and 5.0 MPa H_2. The hydrotreating temperatures varied from 220 to 360 °C, depending on the reactivity of the model compounds. The flow rates of both liquid and gaseous reactants were varied while their ratio was kept constant to obtain reactant conversion and product selectivity at different contact times; this was defined as the ratio of catalyst weight to the molar flow rate of liquid reactant (g_{cat}·h/mol).

Each series of experiments over a fresh catalyst for one specific model compound started with a stabilization period of at least 14 h (overnight) and continued for five days of operation. Each condition was kept over a period of time to reach steady-state. Almost no deactivation of the catalyst was observed, in accordance with less than 5% decrease of reactant conversion and product yields at the same reaction conditions after 120 h time-on-stream (TOS). Selected experiments for each model compound were repeated at least three times at a certain temperature to ensure the standard deviations for the reactant conversion and product yields were less than 10%. The product mass balance ranged from 96% to 102% based on the molar concentration of reactants in the initial feed.

The fresh NiMo/Al_2O_3 catalyst after sulfidation was characterized by N_2 physisorption using the Brunauer–Emmett–Teller (BET) method, inductively coupled plasma optical emission spectrometry (ICP-OES), X-ray photoelectron spectroscopy (XPS), transmission electron microscopy (TEM), and NO chemisorption. The experimental details of all these techniques are provided in the Supporting Information. The chemical composition of all feeds and product mixtures were characterized by gas chromatography for identification (Agilent 7890A GC coupled with mass spectrometry Agilent 5975C MS) and quantification (Shimadzu GC-2010 plus equipped with a flame ionization detector).

3. Results and discussion

Eight different model compounds were selected to represent the nitrogen and oxygen-containing compounds in bio-crudes, as well as sulfur and nitrogen-containing species in petroleum crude oil. Bio-crudes, especially from wet waste such as sewage sludge, contain a significant amount of fatty acid amides, ranging from tetradecanamide to octadecanamide, including mainly primary amides, and also secondary and tertiary amides [37,38]. However, primary amides, such as dodecanamide (DAD), do not dissolve in the nonpolar solvent tetradecane and have a relatively high melting point of 110 °C. Hence, we chose tertiary amide N,N-diethyldodecanamide (DEDAD) and secondary amide N-methyldodecylamine (MDAD) to represent the fatty acid amides. Kinetics of HDN-HDO of DEDAD and MDAD were compared in the absence or presence of H_2S to determine the impact of H_2S. By comparing the kinetics of tertiary amide DMDAD and secondary amide MDAD, the influence of substitution was also discussed.

3.1. Properties of sulfided NiMo/Al_2O_3 catalyst

A sulfided NiMo/Al_2O_3 catalyst was employed for all hydrotreating experiments. Table 2 shows the results of the corresponding

Table 2
BET surface area analysis, ICP-OES, XPS, TEM, and NO chemisorption of the fresh NiMo/Al_2O_3 catalyst.

Characterization	Properties	Fresh NiMo/Al_2O_3 catalyst
BET	Surface area, m^2/g	84.6
	Pore volume, ml/g	0.3
ICP-OES	Ni, wt%	2.43
	Mo, wt%	12.12
	Ni:Mo molar ratio	1:3.1
XPS	Ni:Mo molar ratio	1:3.1
TEM	MoS_2 slab length/nm	3.0
	MoS_2 stacking number	1.9
Chemisorption	NO, μmol/g	100

physicochemical properties. The catalyst had a surface area of 85 m^2/g and a pore volume of 0.3 ml/g. ICP results indicated about 12 wt% Mo and 2.4 wt% Ni on the alumina support with a bulk Ni/Mo molar ratio of 1:3.1 in perfect agreement with the surface Ni/Mo molar ratio determined by XPS, indicating an even distribution of the (Ni)MoS_2 slabs on the Al_2O_3 support. The typical fringes due to MoS_2 crystallites with 0.62–0.65 nm interplanar distances were observed on the TEM micrographs of the sulfided NiMo catalysts (Fig. S3). The stacking number and lengths of at least 200 slabs were measured and the detailed stacking degree and slab length distributions are shown in Fig. S4. Inhomogeneous dispersion of the MoS_2 slabs can be seen with stacking numbers from 1 to 5 layers and lengths between 1 and 6 nm with an average layer stacking and length of 1.9 and 3.0 nm, respectively.

To determine the density of active sites of the sulfide phase in the catalysts, we used both TEM analysis and NO titration. From the TEM data, we used a hexagonal model to correlate the length of the MoS_2 crystallites with the fraction of metal atoms at the edge over the total number of metal atoms [39]. Considering that the Ni-Mo-S structure on the edge is the active domain in the promoted MoS_2 [40], the geometric model indicates that the fraction of metal atoms in the active regions of our catalyst was 0.38. This corresponds to 634 μmol/g metal atoms at the edge position (assuming all Ni atoms are incorporating at the edges). Quantifying the concentration of adsorption sites with chemical titration indicated 100 μmol/g NO adsorbed on the catalyst. This titration has been often used as a measure of active sites, i.e., sulfur vacancies, in sulfide catalysts although the stoichiometry of adsorption, and its reactivity with the sulfide edges, depending on the state of the catalyst [41]. Considering the boundary conditions of one NO molecule per active site and dinitrosyl species formed upon adsorption (two NO molecules per S-vacancy) [42], the concentration of vacancies in our catalyst ranges from 50 to 100 μmol/g. Combining these values with the number of metal sites at edge positions given above, we estimate that the catalyst used in this work has one vacancy per 6.3–12.7 metal atoms at edge positions. This estimate agrees well with the report of one vacancy per ten atoms at the edges of MoS_2, obtained from IR-adsorption spectroscopy of pyridine probe molecules, for a sulfide catalyst with similar composition [43]. Thus, we are confident of the methods that we used in our study to characterize the active phase of the catalyst.

3.2. HDN-HDO of a tertiary amide

The conversion (HDN-HDO) of the tertiary amide DEDAD was tested at 250–280 °C and 5.3 MPa with a contact time up to 64.6 g_{cat}·h/mol. Fig. 1A and B show the partial pressure of reactant and products at different contact times, as well as product selectivity at different DEDAD conversions at 270 °C. Nine products in the liquid phase were observed: N,N-diethyldodecylamine (DEDAM), N-ethyldodecylamine (EDAM), diethylamine, triethylamine, dodecanol, isomers of dodecene (i.e. 2-dodecene, 3-dodecene, and 6-dodecene), dodecane, isomers of undecene (i.e. 1-undecene, 3-undecene, 4-undecene and 5-undecene), and undecane. These products were divided into four categories: amines (DAM, including DEDAM and EDAM), alkanols (dodecanol), C12 alkanes and alkenes, and C11 alkanes and alkenes.

As shown in Fig. 1A, DEDAD reacted rapidly at low contact times (< 20 g_{cat}·h/mol) and its conversion slowed down at higher contact times. DEDAM was the major product with the highest yield at different contact times and showed an initial selectivity of 90% at zero conversion, suggesting it is a primary product from the deoxygenation of DEDAD. The selectivity of DAM slowly declined to 75% with increasing contact time (Fig. 1B), paralleling an increase of C12 selectivity. This indicates that DAM converts to C12 products. To further understand this secondary reaction, the HDN of DMDAM was tested from 270 to 300 °C and 5.3 MPa. The reactant conversion and/or product yield- contact time correlations for the HDN of DMDAM at 270 °C are shown in Fig. 1C. Only C12 products were detected. These results indicate that one pathway for DEDAD conversion starts with deoxygenation to form amine

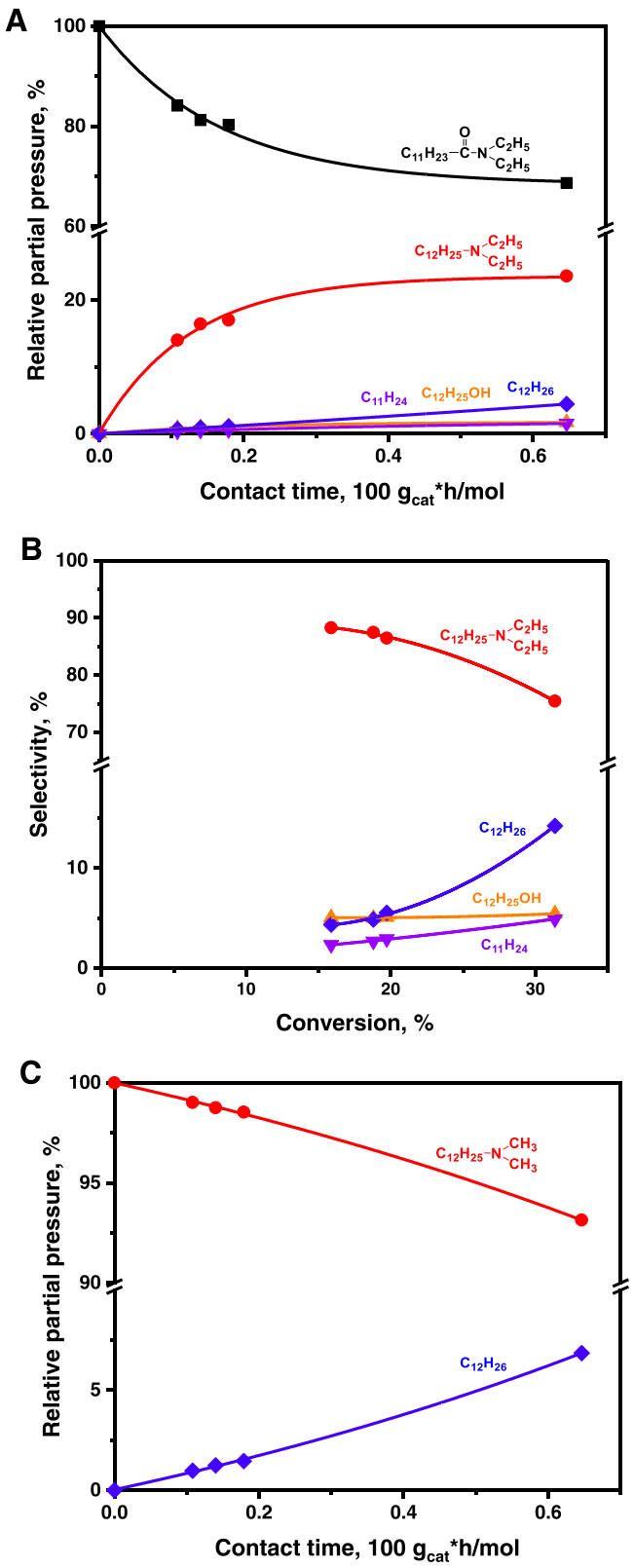

Fig. 1. Conversion (HDO-HDN) of N,N-diethyldodecanamide (DEDAD) and HDN of N,N-dimethyldodecylamine (DMDAM) at 270 °C and 5.0 MPa H_2 on the sulfided NiMo/Al_2O_3 catalysts. (A) The partial pressure of DEDAD and products as a function of contact time. (B) The product selectivity as a function of DEDAD conversion. (C) The partial pressure of DMDAM and product as a function of contact time.

intermediates followed by denitrogenation to yield the final C12 products, as presented in Scheme S1.

Dodecanol was observed with a steady selectivity of around 5% at different contact times, implying that dodecanol is another primary product, formed from direct denitrogenation of DEDAD. C11 and C12 compounds were all observed as non-primary products because of their nearly zero selectivity at initial conversion. It is likely that the conversion of DEDAD to dodecanol proceeds via dodecanal intermediate. As reported in the literature for the HDO of fatty acids [44,45], dodecanoic acid can be hydrogenated to dodecanal, which can be reversibly hydrogenated further to dodecanol with subsequent dehydration to form C12 products without carbon atom loss. Dodecanal can also decarbonylate to produce CO and C11 products. Thus, we propose that DEDAD undergoes C-N bond cleavage to form diethylamine and dodecanal, which is readily converted to C11 or C12 products via dodecanol. However, dodecanal was not detected here, probably because hydrogenation and decarbonylation rates of dodecanal are much faster than its production rate.

The results reveal that HDN-HDO of DEDAD undergoes two parallel reaction pathways, namely deoxygenation (DO) and denitrogenation (DN). The possible reaction network is shown in Scheme 1. In the DO pathway, the oxygen in DEDAD is removed via HDO, i.e., the hydrogenation of the C═O double bond followed by C-O cleavage to eliminate H_2O, resulting in the formation of the primary product DEDAM. This intermediate undergoes the HDN reaction to consecutively cleave the C-N bonds via EDAM and eventually into C12 products. In the DN pathway, the C-N bond cleavage of DEDAD likely forms diethylamine and dodecanal via hydrogenolysis. Then, dodecanal goes through decarbonylation to lose one carbon, leading to the formation of C11 products, or through hydrogenation to form dodecanol, which is deoxygenated to C12 final products.

To calculate the initial rate constants of the two DEDAD conversion pathways, we assumed first-order kinetics and fitted the experimental data at conversion $< 20\%$. Because the H_2 partial pressure in our experiment is in great excess (5.0 MPa for H_2 vs. 10 kPa for initial reactant), we can calculate the initial rate constants of the primary reactions of these reactants by assuming first-order kinetics. We calculated the initial rate constants k (mol/(100 g_{cat}·h)) for the overall conversion of DEDAD and DMDAM and rate constants for the DO (k_{DO}) and DN (k_{DN}) pathways. The values of k are included in Scheme 1. At 270 °C, k_{DO} (1.21 mol/(100 g_{cat}·h)) was almost seven times faster than k_{DN} (0.18 mol/(100 g_{cat}·h)), confirming that DO pathway is the dominating reaction pathway in the HDN-HDO of DEDAD. Similarly, the secondary reaction HDN of DMDAM showed a k_{DMDAM} of 0.086 mol/(100 g_{cat}·h), calculated based on the results in Fig. 1C, which is much lower than k_{DO} of DEDAD. This demonstrates that, in the DO pathway, the primary reaction of DEDAD to the DAM intermediate is much faster than the secondary reaction of DAM to C12 products and the HDN of amines is the rate-limiting step in the HDN-HDO of fatty acid amides. Owing to the rapid DAM formation and slow subsequent consumption, the selectivity of DAM remains the highest as the major product (Fig. 1B). Furthermore, the following discussion shows that DAM at high partial pressure inhibits the DEDAD conversion; this is attributed to the strong adsorption of amines on the catalyst active sites.

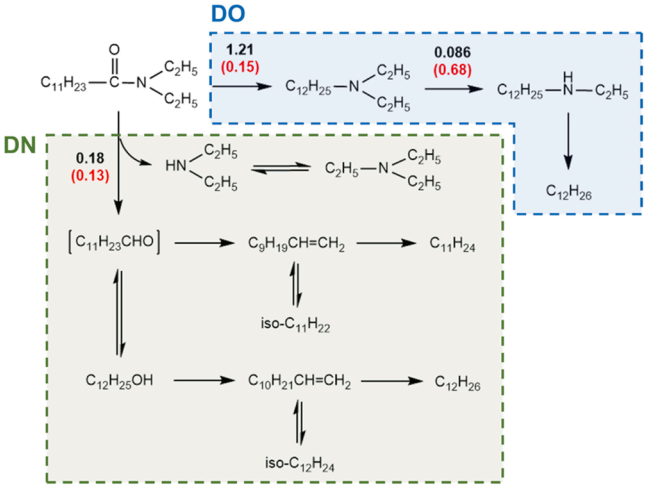

Scheme 1. Reaction pathways in the HDN-HDO of N,N-diethyldodecanamide (DEDAD) and rate constants k (mol/(100 g_{cat}·h)) in the reaction network at 270 °C and 5.0 MPa H_2 in the absence (black numbers above the brackets) and presence (red numbers in the brackets) of 30 kPa H_2S.

3.3. Effect of H_2S on the HDN-HDO of amide

During co-processing, HDS of the sulfur-containing species in petroleum crude oils will produce H_2S, which is known to influence the HDN and HDO kinetics. Here, the effect of H_2S on the HDN-HDO of fatty acid amides was studied in the presence of 30 kPa H_2S. At 5.0 MPa H_2 and 0 kPa H_2S, DEDAD reacted very rapidly (Fig. 1A) and DAM was the main product with high selectivity of at least 75% (Fig. 1B). The addition of 30 kPa H_2S caused a strong decrease in the DEDAD conversion—only 4% at a contact time of 17.9 g_{cat}·h/mol (Fig. 2A) compared to 20% conversion at a similar contact time without H_2S. The product distribution was also different as DAM was not the major product having a selectivity below 20%, as indicated in Fig. 2B. On the contrary, final deoxygenated and denitrogenated C11 and C12 hydrocarbons were the main products with the selectivity of 23% and 63%, respectively, at the highest contact time.

The overall rate constant of DEDAD conversion (k_{DEDAD}) was much lower under 30 kPa H_2S than under 0 kPa (Scheme 1), suggesting H_2S strongly inhibits the conversion of DEDAD. The decrease in k_{DEDAD} was mainly due to the large drop in k_{DO}, which was eight times (0.15 mol/(100 g_{cat}·h)) slower in the presence of 30 kPa H_2S than in the absence of H_2S (1.21 mol/(100 g_{cat}·h), Scheme 1). This demonstrates that H_2S strongly inhibits the deoxygenation of DEDAD. Studies on the impact of H_2S on the deoxygenation of vegetable oils reveal that H_2S inhibited the deoxygenation route in the HDO of rapeseed oil [12]. Contrary to the significant decrease of DAM formation, the yield and selectivity of C12 compounds increased with the presence of H_2S to become the dominant products, changing the major product from DAM to C12. This indicates that H_2S promoted the secondary reaction, i.e., the HDN of DAM in the DO pathway. Therefore, the influence of H_2S on the HDN of DMDAM was verified by introducing 30 kPa H_2S at 270 °C. The presence of H_2S led to a dramatic increase in the DMDAM conversion, up to 36% at the longest contact time with the corresponding growth in the C12 yield (Fig. 2) and the calculated rate constant k_{DMDAM} was about eight times (0.68 mol/(100 g_{cat}·h)) higher in the presence than in the absence of 30 kPa H_2S (Scheme 1). Extensive studies have been conducted previously to investigate the impact of H_2S on HDN reactions. Research on the HDN of quinoline showed that the presence of H_2S significantly increased the reaction rate of quinoline [46]. In addition, Zhang et al. [47] and Satterfield et al. [48] reported that for HDN of indole and pyridine, sulfur compounds had a dual effect on the conversion rate depending on the temperature. The investigation of the HDN of alkylamines mechanism by the Prins research group [49] showed that H_2S has a positive influence on the HDN of amines and acts as a reactant by substituting alkylamines to form alkanethiol intermediates, which is known to be fast over sulfided NiMo/Al_2O_3 catalyst. Together, the inhibition of DEDAD deoxygenation and the promotion of HDN of the intermediate DAM in the DO pathway led to the shift of major products and a low concentration of DAM. This reduced the inhibition in overall DEDAD conversion and hence resulted in a continuous decrease of DEDAD partial pressure with increased contact time (Fig. 2A).

The value of k_{DN} showed only a small change with and without H_2S, decreasing from 0.18 to 0.13 mol/(100 g_{cat}·h) (Scheme 1), indicating

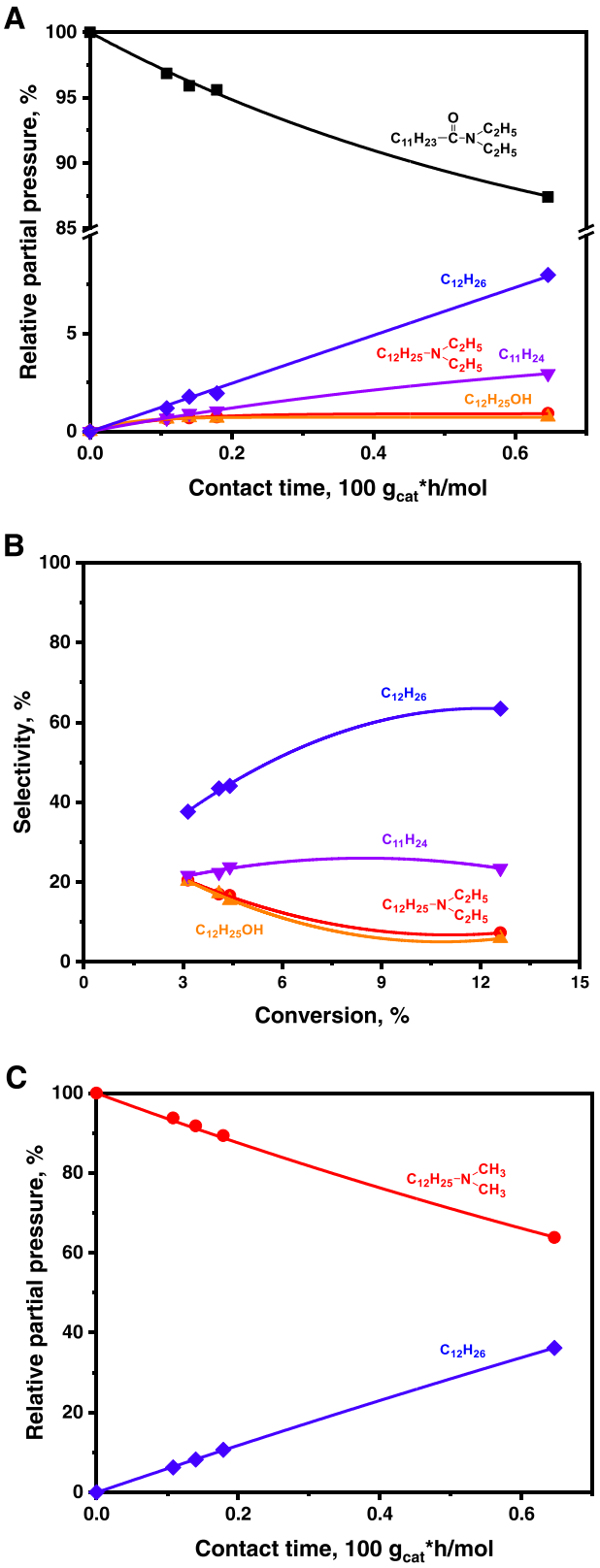

Fig. 2. Conversion (HDN-HDO) of N,N-diethyldodecanamide (DEDAD) and HDN of N,N- dimethyldodecylamine (DMDAM) at 270 °C and 5.0 MPa H_2 on the sulfided $NiMo/Al_2O_3$ catalysts in the presence of 30 kPa H_2S. (A) Partial pressure of DEDAD and products as a function of contact time. (B) Product selectivity as a function of DEDAD conversion. (C) Partial pressure of DMDAM and product as a function of contact time.

that H_2S has little impact on the DN pathway. The influence of H_2S on DN of DEDAD and denitrogenation of DMDAM is different as H_2S showed a strong promotion of HDN of DMDAM but a small inhibition of DN of DEDAD. The apparent activation energy calculation (in Section 3.5) also showed that the denitrogenation of DMDAM has a higher energy barrier than DN of DEDAD. This suggests that the C-N cleavage of the R-CO-N-R linkage in DN of DEDAD has a different reaction mechanism and active site requirement compared to the denitrogenation of regular amines such as DMDAM. Likely, H_2S is not involved as a reactant in the DN of DEDAD. A substantial amount of dodecanol was observed with a selectivity of 20% at the lowest contact time and decreased to 6% with an increasing contact time at 30 kPa H_2S (Fig. 2B). This is in contrast with the constant low selectivity of 5% at 0 kPa H_2S (Fig. 1B), suggesting that H_2S inhibits the conversion of dodecanol to C12 products in the DN pathway. H_2S increased the C11 yield by twice, from 1.5% in the absence of H_2S (Fig. 1A) to 3% in the presence of H_2S (Fig. 2A) at $\tau = 64.6$ g_{cat}·h/mol and improved the corresponding selectivity by nearly five times from 5% (Fig. 1B) to 23% (Fig. 2B). The growths in C11 yield and selectivity reveal that H_2S has a promoting effect on the hydrodecarbonylation reaction. This is plausibly owed to the dissociative adsorption of H_2S on coordinatively unsaturated sites which lead to the formation of functional groups with active roles in the elementary steps of carbon-loss routes [45]. Together, H_2S inhibits the hydrodeoxygenation of dodecanol, but promotes the hydrodecarbonylation of dodecanal. This agrees with literature reports that H_2S has an influence on the HDO process, which could promote the decarboxylation of fatty acids and considerably lower the hydrodeoxygenation/decarboxylation ratio [50].

In summary, H_2S influences the reaction of DEDAD with opposite effects on each reaction step in the reaction network and therefore changes the product distribution. H_2S strongly inhibits the deoxygenation of DEDAD to DAM, which contributes to the major decrease of DEDAD conversions. However, H_2S strongly promotes the HDN of amine intermediates DAM. H_2S also slightly inhibits the denitrogenation of DEDAD to dodecanal and dodecanol intermediates and their further hydrodeoxygenation, but promotes the hydrodecarbonylation of dodecanal.

3.4. HDN-HDO of a secondary amide

The substitution of the amine group influences the HDN of monoalkyl-, dialkyl-, and trialkylamines [51,52]. Similarly, the substitution of the amide group could affect the HDN-HDO chemistry of alkylamides. To discover trends and predict the conversion of primary amide, which is the most abundant nitrogen content in bio-crude, secondary amide MDAD was chosen to compare with the previous tertiary amide DEDAD. We use MDAD, instead of N-ethyldodecanamide, because of the commercial availability issues. However, the impact of the type of alkyl group on the amide reactivity should be slight and we can contribute the reactivity difference between MDAD with DEDAD largely to the difference of substitution degrees. The HDN-HDO of MDAD was performed at 270 °C and 5.3 MPa. Similar to the DEDAD conversion, six products were identified: N-methyldodecylamine (MDAM), dodecanol, dodecenes, dodecane, undecenes, and undecane; which were categorized into the same four groups: amines (DAM, including MDAM), alkanols (dodecanol), C12, and C11 hydrocarbons.

As illustrated in Fig. 3A, the MDAD concentration continuously declined to 64% as the contact time increased. At the same time, DAM yield was always the highest among all the products, up to 27.5% (Fig. 3A). Therefore, DAM became the main product for HDN-HDO of MDAD, similar to the amine intermediate product in the DEDAD conversion. The selectivity of DAM remained the largest and decreased slightly from 88% to 77% during the reaction (Fig. 3B), revealing that DAM derived from the primary reaction of MDAD deoxygenation is a primary product. Comparable to DMDAM conversion, HDN of MDAM was also examined at 270 °C to further verify the secondary reaction of

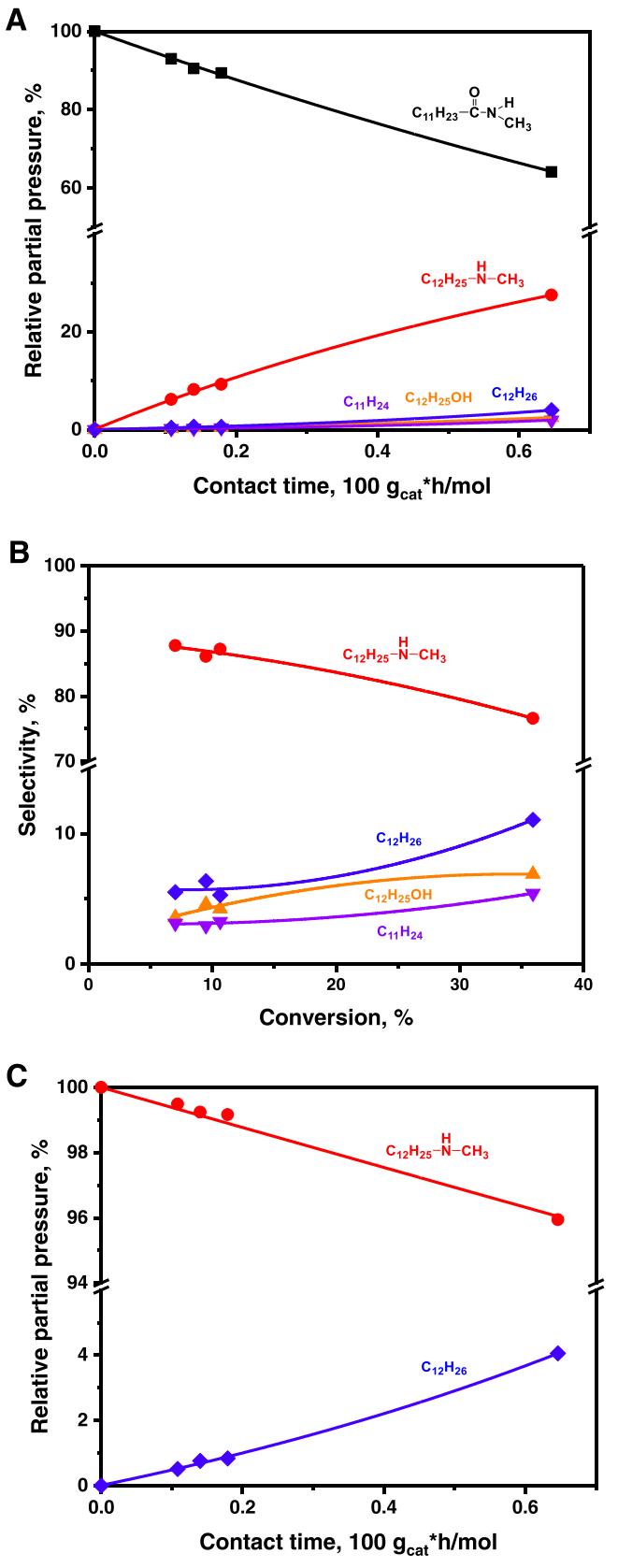

Fig. 3. Conversion (HDN-HDO) of N-methyldodecanamide (MDAD) and HDN of N-methyldodecylamine (MDAM) at 270 °C and 5.0 MPa H_2 on the sulfided $NiMo/Al_2O_3$ catalysts. (A) Partial pressure of MDAD and products as a function of contact time. (B) Product selectivity as a function of MDAD conversion. (C) Partial pressure of MDAM and product as a function of contact time.

DAM intermediate. This produced the same C12 products and the reaction network for HDN of MDAM, as presented in Scheme S2. Likewise, the selectivity of dodecanol ranged from 4% to 7%, following the same reaction network with the DEDAD conversion as a proposed intermediate. Consequently, HDN-HDO of MDAD undertakes the same two reaction pathways (DO and DN) as DEDAD, as shown in Scheme 2.

Furthermore, k_{DO} (0.64 mol/(100 g_{cat}·h)) of MDAD was significantly higher than k_{DN} (0.043 mol/(100 g_{cat}·h)), i.e., about 15 times faster as listed in Scheme 2. This implies that DO is the major reaction pathway for HDN-HDO of MDAD, which is the same conclusion from DEDAD tests. MDAM showed a rate constant of 0.062 mol/(100 g_{cat}·h) (Scheme 2), much lower than k_{DO} of MDAD, indicating that HDN of the DAM intermediate is the rate-determining step in the DO pathway. The similar reaction network and trends of kinetic data for both the secondary and tertiary amides corroborate that these findings are applicable for HDN-HDO of fatty acid amides with similar structures.

When comparing HDN-HDO of the secondary amide with tertiary amide under the same reaction conditions, the overall reaction rate constant k_{MDAD} (0.68 mol/(100 g_{cat}·h)) was only half of k_{DEDAD} (1.39 mol/(100 g_{cat}·h)), implying that tertiary amide reacts faster than secondary amide. Similarly, both k_{DO} and k_{DN} of MDAD were lower than those of DEDAD, which confirms that the reactivity of secondary amide is lower than the tertiary amide. Additionally, k_{MDAM} for HDN of the secondary amine was slower than k_{DMDAM} for HDN of the tertiary amine (Schemes 1 and 2). Besides, the selectivity to DAM from DEDAD (Fig. 1B) dropped slightly more rapidly than that from MDAD (Fig. 3B), implying a quicker conversion of tertiary amine than the secondary amine to final C12 products. Literature shows that for HDN of alkylamines, the conversion increased with increasing basicity of the amine in the order of monoalkylamine < dialkylamine < trialkylamine [53]. Therefore, the substitution of the amide group has an impact on the hydrotreating chemistry of alkylamides, which have higher reactivity with increasing basicity of the amide group. Thus, we can estimate the HDN-HDO activities of all fatty acid amides, such as primary amide, based on the basicity of the amide group.

Fig. 1A shows the conversion of DEDAD initially was fast at a low contact time, then slowed down with minor variation at increasing contact time. Accordingly, the yield of primary product DAM from DEDAD conversion increased rapidly at first and then became stable at a longer contact time. On the contrary, Fig. 3A illustrates that the conversion of MDAD and the DAM yield kept growing gradually until the highest tested contact time. This is because the tertiary amide DEDAD initially converted quicker than the secondary amide MDAD, and thus forming more tertiary amine DEDAM than the secondary amine MDAM.

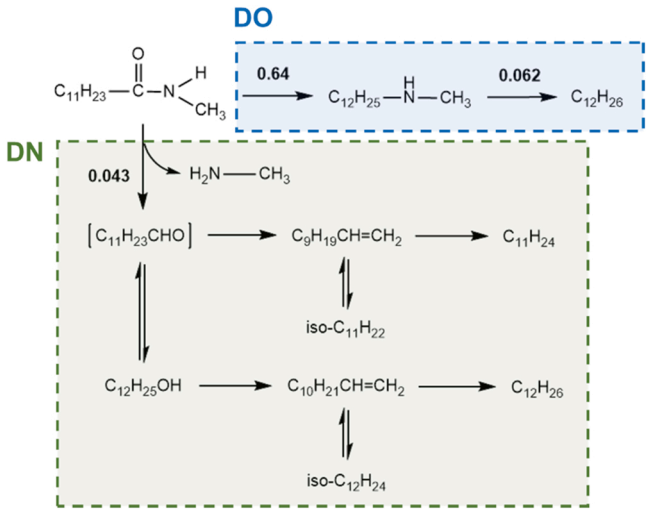

Scheme 2. Reaction pathways in the conversion of MDAD and rate constants k (mol/(100 g_{cat}·h)) in the reaction network at 270 °C and 5.0 MPa H_2.

However, the secondary reaction of HDN of trialkylamine (DEDAM) was faster than the HDN of dialkylamine (MDAM). Hence, there is more DEDAM competing with DEDAD on the accessible active sites and it inhibited the primary reaction of DEDAD conversion. During hydrotreating of alkylamides, the NH_3 and H_2O content formed from HDN-HDO could poison the active sites of the metal sulfide catalysts. [54] However, the reactivity of secondary amide MDAD did not change with time on stream, indicating that there was no catalyst deactivation due to the small amounts of NH_3 or H_2O formed. Thus, it is the amine intermediates that cause the inhibition of tertiary amide DEDAD conversion. This is in line with the basicity of DEDAM, which is stronger than that of MDAM, leading to higher reactivity and stronger product inhibition.

3.5. Kinetics of oxygen-, sulfur- and nitrogen-containing model compounds in co-processing of bio-crudes and petroleum streams

We also determined the kinetics of HDO of dodecanoic acid (DA) and 4-propylphenol which represent other oxygen-containing species of bio-crudes, as well as the HDS of dibenzothiophene (DBT) and HDN of quinoline which represent sulfur and nitrogen species in petroleum crude oil during co-processing. Heterocyclic amines, such as quinoline, are also found in bio-crudes. The reaction networks for each model compound are depicted in Scheme 3.

The catalytic deoxygenation of fatty acids proceeds via two reaction pathways (Scheme 3A): (i) decarboxylation and decarbonylation, which generate CO_2/CO and hydrocarbons with one carbon atom less (DO pathway), and (ii) hydrogenation followed by deoxygenation that produces hydrocarbons of the same carbon numbers (HYD pathway) [44, 55]. HDO of phenolic compounds are proposed to go through two

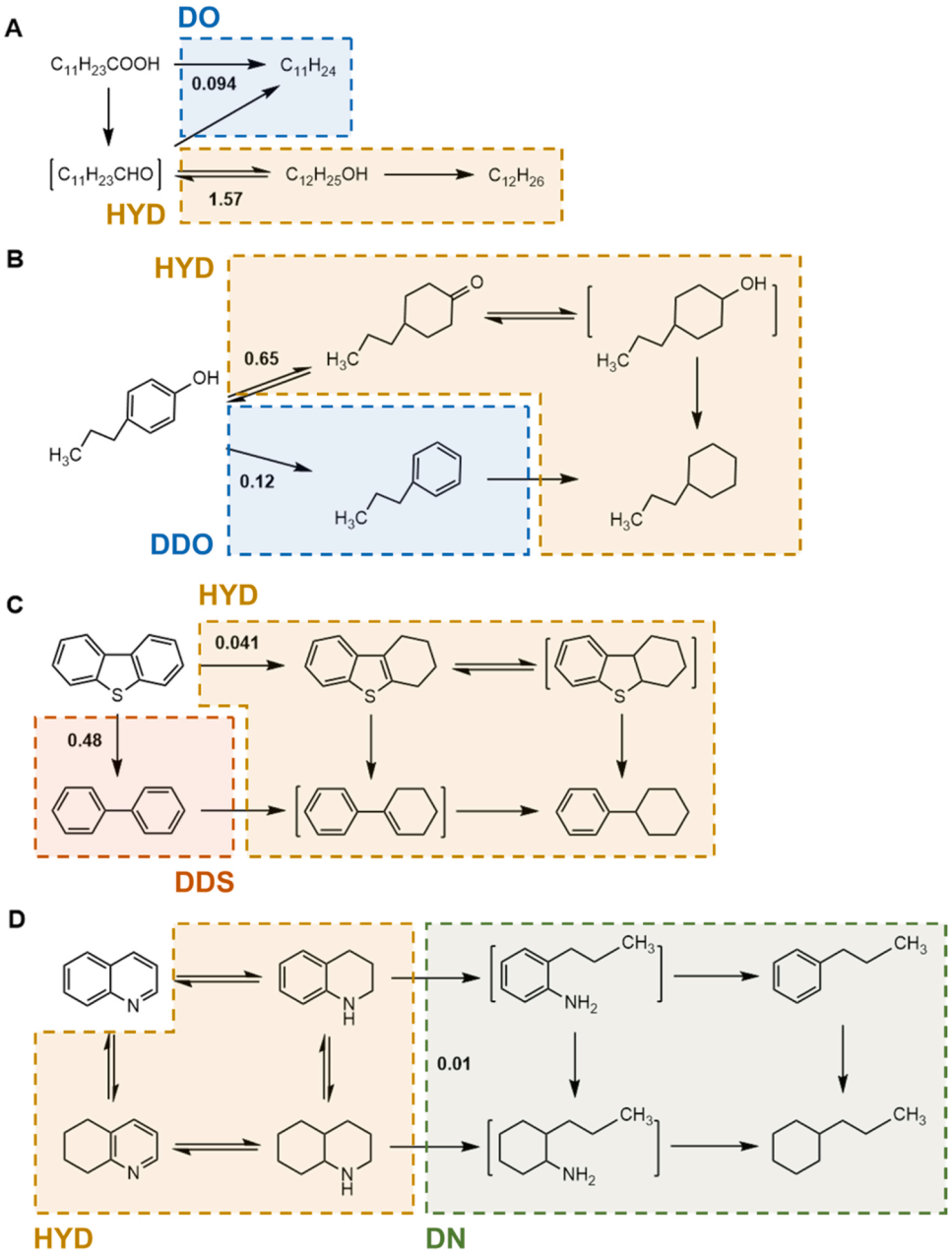

Scheme 3. Reaction pathways in the (A) HDO of dodecanoic acid (DA), (B) HDO of 4-propylphenol, (C) HDS of dibenzothiophene (DBT), and (D) HDN of quinoline as well as rate constants k (mol/(100 g_{cat}·h)) in the reaction network at 270 °C and 5.0 MPa H_2.

competing pathways (Scheme 3B), including direct deoxygenation (DDO pathway) that converts to aromatic compounds, and hydrogenation (HYD pathway) where the benzene ring is hydrogenated first to an oxygen-containing intermediate, then forms final cycloalkanes via deoxygenation [56,57]. Among the most common thiophenes, specifically dibenzothiophene (DBT), its HDS can undergo two reaction pathways (Scheme 3C): direct desulfurization (DDS pathway) or hydrogenation (HYD pathway), which yields sulfur-containing and partially hydrogenated intermediates to be further desulfurized [58,59]. For the pyridinic compounds (Scheme 3D), the hydrogenation (HYD) of the aromatic ring occurs first, either via the benzene ring or the nitrogen-containing heterocycle, followed by subsequent C-N bond cleavage (DN) to bring denitrogenated products [60,61].

Table 3 list the apparent activation energies E_a (kJ/mol), reaction rate constants k (mol/(100 g_{cat}·h)), and the turnover frequencies (TOF, $\times 10^{-2}$ s^{-1}) for different pathways of the nitrogen-, oxygen-, and sulfur-containing model compounds at 270 °C and 5.3 MPa with 10 kPa of the model compound and no H_2S addition. There are several approaches to compare the intrinsic activities of sulfide catalysts by calculating turnover frequencies (TOFs). One approach is to normalize rates with the proportion of promoter atoms at the edges of MoS_2 as determined by TEM and XPS [62]. Another approach is to normalize rates to the concentration of probe molecules that titrate different kinds of active sites in sulfides [63]. Here, TOF was calculated in two ways: the reaction rate constants normalized to the concentration of metal atoms at edge positions (TOF_{edge}, determined by TEM) and the reaction rate constants normalized to the amount of NO adsorbed in the catalysts (TOF_{NO}, determined by NO chemisorption). As shown in Table 3, HDS of DBT showed a TOF_{edge} of 0.23 $\times$ 10^{-2} s^{-1}, which is close to that observed by others over similar NiMo/Al_2O_3 catalysts [64,65].

Most of the overall apparent activation energies of the model compounds that we studied are well above 100 kJ/mol. Fig. 4A shows the overall rate constants for hydrotreating of the nitrogen-, oxygen-, and sulfur-containing model compounds from 250 to 350 °C. The reactivity trend is invariant at low temperature range (< 300 °C), i.e., $k_{DMDAM} < k_{DBT} < k_{4\text{-propylphenol}} < k_{DEDAD} < k_{DA}$. Consequently, HDO of DA and 4-propylphenol displayed higher overall rate constants than HDS of DBT and HDN of DMDAM, illustrating that HDO and HDS are easier than HDN over the sulfided NiMo catalyst. The values of overall rate constants at 270 °C in Table 3 are consistent with this trend. The overall apparent activation energy of DA is 88 kJ/mol. Thus, it has the highest reactivity at low temperatures but becomes less reactive as the temperature increases (Fig. 4A). However, this reactivity trend holds only for the overall conversion of these model compounds.

Fig. 4B indicates that DEDAD has a higher rate constant than DMDAM at low temperatures, but it turns to less reactive than DMDAM above 300 °C. This is because the apparent activation energy for the denitrogenation of DMDAM (146 kJ/mol) is much higher than DN of DEDAD (81 kJ/mol), as listed in Table 3. It suggests breaking the C-N bond in a tertiary amine (DMDAM) has a higher intrinsic energy barrier than that in an amide (DEDAD). The DN reactivity of quinoline remains the lowest over a wide temperature range from 250 to 350 °C. At 270 °C, k_{DN} of quinoline was merely 0.01 mol/(100 g_{cat}·h), far lower than that of DMDAM (Table 3). This is likely because the C-N bond cleavage for HDN of quinoline is the secondary step occurring after hydrogenation of the aromatic ring. In contrast, nitrogen removal for HND of DMDAM is the primary step. Regardless, the relatively sluggish kinetics of nitrogen removal and the strong inhibition effect of nitrogenous compounds on other reactions indicates that HDN is critical for heteroatom removal in co-processing considering the high N content in bio-crude. For instance, a 10% blending of a typical bio-crude to refinery stream, such as VGO, will lead to an increase of nitrogen content by 4000–9000 ppm.

Concerning the direct removal of oxygen, DEDAD is the most reactive molecule followed by 4-propylphenol and DA in the temperature range from 250 to 350 °C, as shown in Fig. 4C. The high activation energy for DO pathway of 4-propylphenol (179 kJ/mol) makes it shift from the least to the most reactive molecule for direct oxygen removal as temperature increasing. The slow rate constant k_{DO} of DA has a positive implication since the DO pathway leads to one carbon loss in the form of CO_x. Furthermore, k_{DDS} of DBT was noticeably larger than k_{DO} of DA and 4-propylphenol at low temperatures, indicating that the NiMo sulfide catalyst is better at direct sulfur removal than at direct oxygen removal. These comparisons imply that although HTL bio-crudes are high in oxygen-containing compounds (Table 1), such as fatty acids or phenols, HDO may not be a significant issue in co-processing compared to HDN of nitrogenous species.

The k_{DO} values of DA and 4-propylphenol were considerably lower than the corresponding k_{HYD} values (Fig. 4C and D). Thus, DA and 4-propylphenol preferentially react through the HYD pathway, which leads to deoxygenated hydrocarbons via hydrogenated intemediates (Scheme 3A and B). On the other hand, k_{DDS} of DBT was substantially higher than k_{HYD} at a broad temperature range, indicating HDS of DBT preferentially reacts through the direct sulfur removal, e.g., k_{DDS} of DBT is 0.48 mol/(100 g_{cat}·h)), while k_{HYD} is merely 0.04 mol/(100 g_{cat}·h) at 270 °C.

We acknowledge that this discussion does not consider the competitive adsorption among different species. Introducing bio-crudes into a refinery hydrotreater with petroleum streams, such as VGO, will lead to inhibition of HDS because of the strong adsorption of amines. Together with the slow kinetics of nitrogen removal, hydrotreating process and catalyst improvement will be required to mitigate the impacts of nitrogenous species when co-processing HTL bio-crudes in the current refinery. Both aspects are the topics of ongoing work.

4. Conclusion

This work reports the kinetics and reaction network of hydrodenitrogenation-hydrodeoxygenation (HDN-HDO) of N,N-diethyldodecanamide (DEDAD) and N-methyldodecanamide (MDAD) as model compounds for alkylamides, major nitrogen and oxygen-containing components in HTL bio-crudes. A fixed-bed, continuous reactor and a NiMo sulfide catalyst were employed for the hydrotreating tests. The conversion of DEDAD and MDAD undergoes two reaction

Table 3
Apparent activation energies E_a (kJ/mol), first-order rate constants k (mol/(100 g_{cat}·h)), and turnover frequency TOF values ($\times 10^{-2}$ s^{-1}) for the nitrogen-, oxygen-, and sulfur-containing model compounds over NiMo sulfide catalyst at 270 °C and 5.3 MPa with 10 kPa of the model compound and no H_2S addition.

Model compound	E_a (kJ/mol)			k (mol/ (100 g_{cat}·h))			TOF_{NO} ($\times 10^{-2}$ s^{-1})	TOF_{edge} ($\times 10^{-2}$ s^{-1})
N-containing	**overall**	**DO**	**DN**	**overall**	**DO**	**DN**	**overall**	**overall**
DEDAD	111.6 ± 15.1	117.1 ± 15.5	81.3 ± 19.2	1.39	1.21	0.18	3.86	0.61
DMDAM	146.0 ± 9.9		146.0 ± 9.9	0.09		0.09	0.25	0.04
Quinoline[a]			81.0 ± 10.3			0.01		
O-containing	**overall**	**DO**	**HYD**	**overall**	**DO**	**HYD**	**overall**	**overall**
DA[a]	88.4 ± 9.3	107.3 ± 13.6	87.3 ± 9.1	1.66	0.09	1.57	4.61	0.73
4-Propylphenol[a]	117.7 ± 5.7	178.8 ± 7.9	111.6 ± 6.1	0.77	0.12	0.65	2.14	0.34
S-containing	**overall**	**DDS**	**HYD**	**overall**	**DDS**	**HYD**	**overall**	**overall**
DBT	117.9 ± 1.7	117.2 ± 1.8	127.6 ± 20.7	0.52	0.48	0.04	1.44	0.23

[a] First-order rate constants k (mol/(100 g_{cat}·h)) for the HDO of DA, 4-propylphenol, and HDN of quinoline were calculated by extrapolation at 270 °C.

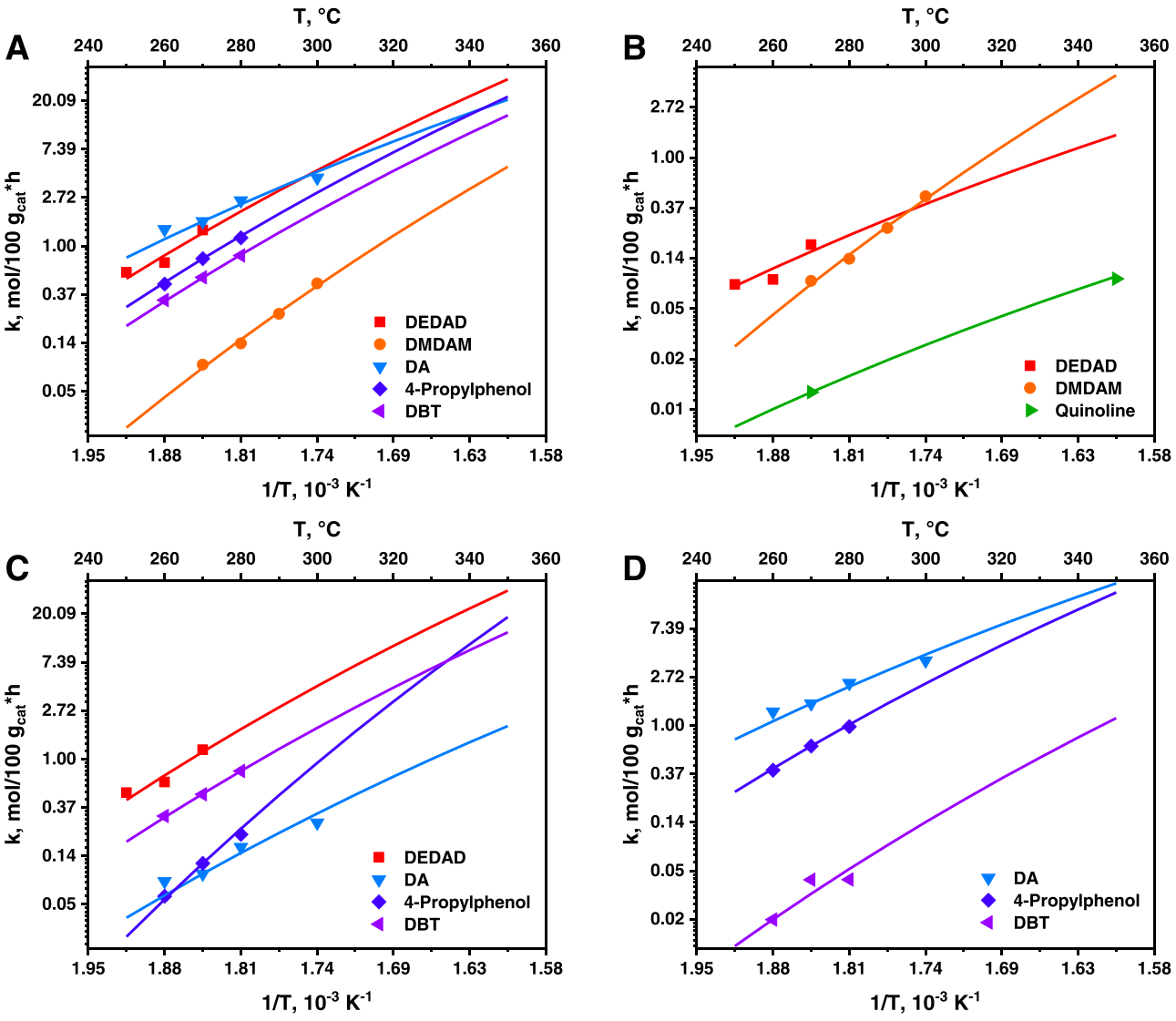

Fig. 4. Reaction rate constants of (A) the overall conversion, (B) DN pathways, (C) DO and DDS pathways, and (D) HYD pathways from 250 to 350 °C for the nitrogen-, oxygen-, and sulfur-containing model compounds over NiMo sulfide catalyst.

pathways, namely deoxygenation (DO) and denitrogenation (DN). The DO pathway starts with the HDO of the C═O bond to form an amine intermediate. The DN pathway initiates with the C-N bond rupture to produce one mole of small amine molecule and one mole of alkanol intermediate. Our results showed that the DO pathway had much higher rate constants than the DN pathway. Within the DO pathway, the subsequent HDN of amines is more difficult than the initial deoxygenation of alkylamides, showing that nitrogen removal will be the limiting step for complete defunctionalization. The presence of H_2S significantly suppressed the fatty acid amide conversion and especially inhibited the DO pathway, but strongly promoted secondary reaction of HDN of amines. The secondary amide MDAD converted slower than tertiary amide DEDAD under the same reaction conditions due to the basicity of the amide group. Comparison of the kinetics of several model compounds standing for the heteroatom-containing species in bio-crudes and petroleum streams indicate that removal of oxygen (dodecanoic acid, 4-propylphenol) and sulfur (dibenzothiophene) are faster than the removal of nitrogen (amides, amines, and quinoline).

CRediT authorship contribution statement

Cheng Zhu: Methodology, Investigation, Data curation, Writing – original draft. **Oliver Y. Gutiérrez:** Methodology, Visualization, Writing – review & editing. **Daniel M. Santosa:** Methodology, Experimentation. **Matthew Flake:** Experimentation, Data curation. **Roland Weindl:** Experimentation, Data curation. **Igor Kutnyakov:** Experimentation, Data curation. **Hui Shi:** Methodology, Data curation. **Huamin Wang:** Conceptualization, Writing – review & editing, Supervision, Funding acquisition.

Declaration of Competing Interest

The authors declare that they have no known competing financial interests or personal relationships that could have appeared to influence the work reported in this paper.

Acknowledgements

The authors gratefully acknowledge funding for this research, provided by the U.S. Department of Energy (DOE), Office of Energy Efficiency and Renewable Energy (EERE), Bioenergy Technologies Office (BETO). This work was performed at the Pacific Northwest National Laboratory (PNNL), which is operated for the U.S. Department of Energy by Battelle under Contract DE-AC06-76RL0183. The authors also thank

Professor J.A. Lercher for providing laboratory facilities for the characterization of sulfide materials at the Catalysis Research Center in the Technische Universität München. The views and opinions of the authors expressed herein do not necessarily state or reflect those of the U.S. Government or any agency thereof. Neither the U.S. Government nor any agency thereof, nor any of their employees, makes any warranty, expressed or implied, or assumes any legal liability or responsibility for the accuracy, completeness, or usefulness of any information, apparatus, product, or process disclosed, or represents that its use would not infringe privately owned rights.

Appendix A. Supporting information

Supplementary data associated with this article can be found in the online version at doi:10.1016/j.apcatb.2022.121197.

References

[1] S. Hansen, A. Mirkouei, L.A. Diaz, A comprehensive state-of-technology review for upgrading bio-oil to renewable or blended hydrocarbon fuels, Renew. Sustain. Energy Rev. 118 (2020), 109548.
[2] A. Abdulkareem, M. Asikin, Lee, Rashid, Islam, Y. Taufiq, A review on thermal conversion of plant oil (edible and inedible) into green fuel using carbon-based nanocatalyst, Catalysts 9 (2019) 350.
[3] M.B. Griffin, K. Iisa, H. Wang, A. Dutta, K.A. Orton, R.J. French, D.M. Santosa, N. Wilson, E. Christensen, C. Nash, K.M. Van Allsburg, F.G. Baddour, D.A. Ruddy, E.C.D. Tan, H. Cai, C. Mukarakate, J.A. Schaidle, Driving towards cost-competitive biofuels through catalytic fast pyrolysis by rethinking catalyst selection and reactor configuration, Energy Environ. Sci. 11 (2018) 2904–2918.
[4] K. Jacobson, K.C. Maheria, A. Kumar Dalai, Bio-oil valorization: a review, Renew. Sustain. Energy Rev. 23 (2013) 91–106.
[5] F. Cheng, Z. Cui, L. Chen, J. Jarvis, N. Paz, T. Schaub, N. Nirmalakhandan, C. E. Brewer, Hydrothermal liquefaction of high- and low-lipid algae: Bio-crude oil chemistry, Appl. Energy 206 (2017) 278–292.
[6] I. Nava Bravo, S.B. Velásquez-Orta, R. Cuevas-García, I. Monje-Ramírez, A. Harvey, M.T. Orta Ledesma, Bio-crude oil production using catalytic hydrothermal liquefaction (HTL) from native microalgae harvested by ozone-flotation, Fuel 241 (2019) 255–263.
[7] D.R. Vardon, B.K. Sharma, J. Scott, G. Yu, Z. Wang, L. Schideman, Y. Zhang, T. J. Strathmann, Chemical properties of biocrude oil from the hydrothermal liquefaction of Spirulina algae, swine manure, and digested anaerobic sludge, Bioresour. Technol. 102 (2011) 8295–8303.
[8] S.-Y. Chen, T. Mochizuki, M. Nishi, H. Takagi, Y. Yoshimura, M. Toba, Hydrotreating of Jatropha-derived bio-oil over mesoporous sulfide catalysts to produce drop-in transportation fuels, Catalysts 9 (2019) 392.
[9] S.T. Oyama, X. Wang, F.G. Requejo, T. Sato, Y. Yoshimura, Hydrodesulfurization of petroleum feedstocks with a new type of nonsulfide hydrotreating catalyst, J. Catal. 209 (2002) 1–5.
[10] J.M. Jarvis, K.O. Albrecht, J.M. Billing, A.J. Schmidt, R.T. Hallen, T.M. Schaub, Assessment of hydrotreatment for hydrothermal liquefaction biocrudes from sewage sludge, microalgae, and pine feedstocks, Energy Fuels 32 (2018) 8483–8493.
[11] S. van Dyk, J. Su, J.D. McMillan, J. Saddler, Potential synergies of drop-in biofuel production with further co-processing at oil refineries, Biofuels Bioprod. Bioref. 13 (2019) 760–775.
[12] A.N. Varakin, A.V. Mozhaev, A.A. Pimerzin, P.A. Nikulshin, Toward HYD/DEC selectivity control in hydrodeoxygenation over supported and unsupported Co(Ni)-MoS2 catalysts. A key to effective dual-bed catalyst reactor for co-hydroprocessing of diesel and vegetable oil, Catal. Today 357 (2020) 556–564.
[13] A.H. Zacher, D.C. Elliott, M.V. Olarte, H. Wang, S.B. Jones, P.A. Meyer, Technology advancements in hydroprocessing of bio-oils, Biomass Bioenergy 125 (2019) 151–168.
[14] B.S. Rana, R. Kumar, R. Tiwari, R. Kumar, R.K. Joshi, M.O. Garg, A.K. Sinha, Transportation fuels from co-processing of waste vegetable oil and gas oil mixtures, Biomass Bioenergy 56 (2013) 43–52.
[15] D. Sági, P. Baladincz, Z. Varga, J. Hancsók, Co-processing of FCC light cycle oil and waste animal fats with straight run gas oil fraction, J. Clean. Prod. 111 (2016) 34–41.
[16] S. Bezergianni, A. Dimitriadis, Temperature effect on co-hydroprocessing of heavy gas oil–waste cooking oil mixtures for hybrid diesel production, Fuel 103 (2013) 579–584.
[17] S. Badoga, A. Alvarez-Majmutov, T. Xing, R. Gieleciak, J. Chen, Co-processing of hydrothermal liquefaction biocrude with vacuum gas oil through hydrotreating and hydrocracking to produce low-carbon fuels, Energy Fuels 34 (2020) 7160–7169.
[18] R.L. Ware, R.P. Rodgers, A.G. Marshall, O.D. Mante, D.C. Dayton, S. Verdier, J. Gabrielsen, S.M. Rowland, Tracking elemental composition through hydrotreatment of an upgraded pyrolysis oil blended with a light gas oil, Energy Fuels 34 (2020) 16181–16186.
[19] A. Alvarez-Majmutov, S. Badoga, J. Chen, J. Monnier, Y. Zhang, Co-processing of deoxygenated pyrolysis bio-oil with vacuum gas oil through hydrocracking, Energy Fuels 35 (2021) 9983–9993.
[20] R.B. Madsen, H. Zhang, P. Biller, A.H. Goldstein, M. Glasius, Characterizing semivolatile organic compounds of biocrude from hydrothermal liquefaction of biomass, Energy Fuels 31 (2017) 4122–4134.
[21] S. Chiaberge, I. Leonardis, T. Fiorani, G. Bianchi, P. Cesti, A. Bosetti, M. Crucianelli, S. Reale, F. De Angelis, Amides in bio-oil by hydrothermal liquefaction of organic wastes: a mass spectrometric study of the thermochemical reaction products of binary mixtures of amino acids and fatty acids, Energy Fuels 27 (2013) 5287–5297.
[22] O. Palardy, C. Behnke, L.M.L. Laurens, Fatty amide determination in neutral molecular fractions of green crude hydrothermal liquefaction oils from algal biomass, Energy Fuels 31 (2017) 8275–8282.
[23] W. Costanzo, R. Hilten, U. Jena, K.C. Das, J.R. Kastner, Effect of low temperature hydrothermal liquefaction on catalytic hydrodenitrogenation of algae biocrude and model macromolecules, Algal Res. 13 (2016) 53–68.
[24] I. Hita, S.M. Sarathy, P. Castaño, Polymeric waste valorization at a crossroads: ten ways to bridge the research on model and complex/real feedstock, Green Chem. 23 (2021) 4656–4664.
[25] C. Zhao, J. He, A.A. Lemonidou, X. Li, J.A. Lercher, Aqueous-phase hydrodeoxygenation of bio-derived phenols to cycloalkanes, J. Catal. 280 (2011) 8–16.
[26] S. Leng, X. Wang, X. He, L. Liu, Ye Liu, X. Zhong, G. Zhuang, J.-g Wang, NiFe/γ-Al2O3: a universal catalyst for the hydrodeoxygenation of bio-oil and its model compounds, Catal. Commun. 41 (2013) 34–37.
[27] H. Wang, R. Prins, Hydrodesulfurization of dibenzothiophene and its hydrogenated intermediates over sulfided Mo/γ-Al2O3, J. Catal. 258 (2008) 153–164.
[28] P.G. Moses, B. Hinnemann, H. Topsøe, J.K. Nørskov, The effect of Co-promotion on MoS2 catalysts for hydrodesulfurization of thiophene: a density functional study, J. Catal. 268 (2009) 201–208.
[29] S. Albersberger, H. Shi, M. Wagenhofer, J. Han, O.Y. Gutiérrez, J.A. Lercher, On the enhanced catalytic activity of acid-treated, trimetallic Ni-Mo-W sulfides for quinoline hydrodenitrogenation, J. Catal. 380 (2019) 332–342.
[30] L. Qu, M. Flechsenhar, R. Prins, Kinetics of the hydrodenitrogenation of o-toluidine over fluorinated NiMoS/Al2O3 and NiMoS/ASA catalysts, J. Catal. 217 (2003) 284–291.
[31] M. Liu, Y. Shi, K. Wu, J. Liang, Y. Wu, S. Huang, M. Yang, Upgrading of palmitic acid and hexadecanamide over Co-based catalysts: Effect of support (SiO2, γ-Al2O3 and H-ZSM-22), Catal. Commun. 129 (2019), 105726.
[32] J. Cheng, R. Huang, T. Yu, T. Li, J. Zhou, K. Cen, Biodiesel production from lipids in wet microalgae with microwave irradiation and bio-crude production from algal residue through hydrothermal liquefaction, Bioresour. Technol. 151 (2014) 415–418.
[33] P. Biller, B.K. Sharma, B. Kunwar, A.B. Ross, Hydroprocessing of bio-crude from continuous hydrothermal liquefaction of microalgae, Fuel 159 (2015) 197–205.
[34] M. Lavanya, A. Meenakshisundaram, S. Renganathan, S. Chinnasamy, D.M. Lewis, J. Nallasivam, S. Bhaskar, Hydrothermal liquefaction of freshwater and marine algal biomass: a novel approach to produce distillate fuel fractions through blending and co-processing of biocrude with petrocrude, Bioresour. Technol. 203 (2016) 228–235.
[35] Y. Hu, M. Gong, S. Feng, C. Xu, A. Bassi, A review of recent developments of pre-treatment technologies and hydrothermal liquefaction of microalgae for bio-crude oil production, Renew. Sustain. Energy Rev. 101 (2019) 476–492.
[36] H. Wang, S.-J. Lee, M.V. Olarte, A.H. Zacher, Bio-oil stabilization by hydrogenation over reduced metal catalysts at low temperatures, ACS Sustain. Chem. Eng. 4 (2016) 5533–5545.
[37] D. Castello, M.S. Haider, L.A. Rosendahl, Catalytic upgrading of hydrothermal liquefaction biocrudes: Different challenges for different feedstocks, Renew. Energy 141 (2019) 420–430.
[38] X. Tang, C. Zhang, Z. Li, X. Yang, Element and chemical compounds transfer in bio-crude from hydrothermal liquefaction of microalgae, Bioresour. Technol. 202 (2016) 8–14.
[39] S. Shan, P. Yuan, W. Han, G. Shi, X. Bao, Supported NiW catalysts with tunable size and morphology of active phases for highly selective hydrodesulfurization of fluid catalytic cracking naphtha, J. Catal. 330 (2015) 288–301.
[40] E.J.M. Hensen, P.J. Kooyman, Y. van der Meer, A.M. van der Kraan, V.H.J. de Beer, J.A.R. van Veen, R.A. van Santen, The relation between morphology and hydrotreating activity for supported MoS2 particles, J. Catal. 199 (2001) 224–235.
[41] A. Hrabar, J. Hein, O.Y. Gutiérrez, J.A. Lercher, Selective poisoning of the direct denitrogenation route in o-propylaniline HDN by DBT on Mo and NiMo/γ-Al2O3 sulfide catalysts, J. Catal. 281 (2011) 325–338.
[42] N. Koizumi, S. Jung, Y. Hamabe, H. Suzuki, M. Yamada, Investigation of surface site of Ni species on NiMo/Al2O3 hydrodesulfurization catalyst sulfided at high-pressure by means of DRIFTS combined with low-temperature NO adsorption, Catal. Lett. 135 (2010) 175–181.
[43] E. Schachtl, E. Kondratieva, O.Y. Gutierrez, J.A. Lercher, Pathways for H2 activation on (Ni)-MoS2 catalysts, J. Phys. Chem. Lett. 6 (2015) 2929–2932.
[44] L. Hermida, A.Z. Abdullah, A.R. Mohamed, Deoxygenation of fatty acid to produce diesel-like hydrocarbons: a review of process conditions, reaction kinetics and mechanism, Renew. Sustain. Energy Rev. 42 (2015) 1223–1233.
[45] M.F. Wagenhofer, E. Baráth, O.Y. Gutiérrez, J.A. Lercher, Carbon–carbon bond scission pathways in the deoxygenation of fatty acids on transition-metal sulfides, ACS Catal. 7 (2017) 1068–1076.

[46] H. Farag, M. Kishida, H. Al-Megren, Competitive hydrodesulfurization of dibenzothiophene and hydrodenitrogenation of quinoline over unsupported MoS2 catalyst, Appl. Catal. A Gen. 469 (2014) 173–182.
[47] L. Zhang, U.S. Ozkan, Hydrodenitrogenation of indole over NiMo sulfide catalysts, Stud. Surf. Sci. Catal. 101 (1996) 1223–1232.
[48] W. Kanda, I. Siu, J. Adjaye, A.E. Nelson, M.R. Gray, Inhibition and deactivation of hydrodenitrogenation (HDN) Catalysts by narrow-boiling fractions of athabasca coker gas oil, Energy Fuels 18 (2004) 539–546.
[49] Y. Zhao, R. Prins, Mechanisms of hydrodenitrogenation of alkylamines and hydrodesulfurization of alkanethiols on NiMo/Al2O3, CoMo/Al2O3, and Mo/Al2O3, J. Catal. 229 (2005) 213–226.
[50] S. Chen, Green oil production by hydroprocessing, Int. J. Clean. Coal Energy 01 (2012) 43–55.
[51] N. Sivasankar, R. Prins, Iminium cations as intermediates in the hydrodenitrogenation of alkylamines over sulfided NiMo/γ-Al2O3, Catal. Today 116 (2006) 542–553.
[52] R. Prins, Y. Zhao, N. Sivasankar, P. Kukula, Mechanism of CN bond breaking in hydrodenitrogenation, J. Catal. 234 (2005) 509–512.
[53] Y. Zhao, P. Kukula, R. Prins, Investigation of the mechanism of the hydrodenitrogenation of n-hexylamines over sulfided NiMo/γ-Al2O3, J. Catal. 221 (2004) 441–454.
[54] H. Ohta, B. Feng, H. Kobayashi, K. Hara, A. Fukuoka, Selective hydrodeoxygenation of lignin-related 4-propylphenol into n-propylbenzene in water by Pt-Re/ZrO2 catalysts, Catal. Today 234 (2014) 139–144.
[55] P. Kumar, S.R. Yenumala, S.K. Maity, D. Shee, Kinetics of hydrodeoxygenation of stearic acid using supported nickel catalysts: effects of supports, Appl. Catal. A Gen. 471 (2014) 28–38.
[56] C. Chen, G. Chen, F. Yang, H. Wang, J. Han, Q. Ge, X. Zhu, Vapor phase hydrodeoxygenation and hydrogenation of m -cresol on silica supported Ni, Pd and Pt catalysts, Chem. Eng. Sci. 135 (2015) 145–154.
[57] S. Salakhum, T. Yutthalekha, S. Shetsiri, T. Witoon, C. Wattanakit, Bifunctional and bimetallic Pt–Ru/HZSM-5 nanoparticles for the mild hydrodeoxygenation of lignin-derived 4-propylphenol, ACS Appl. Nano Mater. 2 (2019) 1053–1062.
[58] M.A. Alamoudi, K.J. Smith, Hydrodesulphurization of dibenzothiophene on NiMoS catalysts: Impact of the carbon support on the reaction kinetics, Can. J. Chem. Eng. 97 (2019) 1496–1505.
[59] M. Philippe, F. Richard, D. Hudebine, S. Brunet, Inhibiting effect of oxygenated model compounds on the HDS of dibenzothiophenes over CoMoP/Al2O3 catalyst, Appl. Catal. A Gen. 383 (2010) 14–23.
[60] J. Liu, W.-y Li, J. Feng, X. Gao, Z.-y Luo, Promotional effect of TiO2 on quinoline hydrodenitrogenation activity over Pt/γ-Al2O3 catalysts, Chem. Eng. Sci. 207 (2019) 1085–1095.
[61] Y. Luan, Q. Zhang, D. He, J. Guan, C. Liang, Hydrodenitrogenation of quinoline and its intermediates over sulfided NiW/γ-Al2O3 in the absence and presence of H2S, Asia Pac. J. Chem. Eng. 4 (2009) 704–710.
[62] P.P. Minaev, P.A. Nikulshin, M.S. Kulikova, A.A. Pimerzin, V.M. Kogan, NiWS/Al2O3 hydrotreating catalysts prepared with 12-tungstophosphoric heteropolyacid and nickel citrate: effect of Ni/W ratio, Appl. Catal. A Gen. 505 (2015) 456–466.
[63] M. Wagenhofer, H. Shi, O. Gutierrez, A. Jentys, J. Lercher, Enhancing hydrogenation activity of Ni-Mo sulfide hydrodesulfurization catalysts, Sci. Adv. 6 (2020) eaax5331.
[64] W. Lai, W. Song, L. Pang, Z. Wu, N. Zheng, J. Li, J. Zheng, X. Yi, W. Fang, The effect of starch addition on combustion synthesis of NiMo–Al2O3 catalysts for hydrodesulfurization, J. Catal. 303 (2013) 80–91.
[65] A.S. Koklyukhin, A.V. Mozhaev, V.A. Sal'nikov, P.A. Nikul'shin, Promoter nature effect on the sensitivity of Ni–Mo/Al2O3, Co–Mo/Al2O3, and Ni–Co–Mo/Al2O3 catalysts to dodecanoic acid in the co-hydrotreating of dibenzothiophene and naphthalene, Kinet. Catal. 58 (2017) 463–470.